Ligand Binding-Induced Conformational Changes in Riboflavin Kinase: Structural Basis for the Ordered Mechanism[†,‡]

Subramanian Karthikeyan,[§] Qingxian Zhou,[§] Andrei L. Osterman,[||] and Hong Zhang*[,§]

Department of Biochemistry, University of Texas Southwestern Medical Center, Dallas, Texas 75390, and Integrated Genomics, Inc., Chicago, Illinois 60612

Received August 13, 2003; Revised Manuscript Received September 3, 2003

ABSTRACT: Riboflavin kinase (RFK) is an essential enzyme catalyzing the phosphorylation of riboflavin (vitamin B_2) in the presence of ATP and Mg^{2+} to form the active cofactor FMN, which can be further converted to FAD. Previously, the crystal structures of RFKs from human and *Schizosaccharomyces pombe* have been determined in the apo form and in complex with MgADP. These structures revealed that RFK adopts a novel kinase fold and utilizes a unique nucleotide binding site. The structures of the flavin-bound RFK obtained by soaking pre-existing crystals were also reported. Because of crystal packing restraints, these flavin-bound RFK complexes adopt conformations nearly identical with that of corresponding flavin-free structures. Here we report the structure of human RFK cocrystallized with both MgADP and FMN. Drastic conformational changes associated with flavin binding are observed primarily at the so-called Flap I and Flap II loop regions. As a result, the bound FMN molecule now interacts with the enzyme extensively and is well-ordered. Residues from Flap II interact with Flap I and shield the FMN molecule from the solvent. The conformational changes in Flap I resulted in a new Mg^{2+} coordination pattern in which a FMN phosphate oxygen and Asn36 side chain carbonyl are directly coordinating to the Mg^{2+} ion. The proposed catalytic base Glu86 is well-positioned for activation of the O5′ hydroxyl group of riboflavin for the phosphoryl transfer reaction. The structural data obtained so far on human and yeast RFK complexes provide a rationale for the ordered kinetic mechanism of RFK.

Riboflavin kinase (RFK)[1] catalyzes the obligatory step in the flavin cofactor biosynthesis in all organisms. It phosphorylates riboflavin to form flavin mononucleotide (FMN) in the presence of ATP and Mg^{2+} or other divalent ions. The product FMN can be further converted to flavin adenine dinucleotide (FAD) by FMN adenylyltransferase (FMNAT) (*1*). In bacteria, both functions of RFK and FMNAT are encoded in a single bifunctional enzyme FAD synthase (FADS), the protein product of the *ribF* or *ribC* gene (*2*, *3*). In eukaryotes (from yeast to humans), RFK and FMNAT exist as separate monofunctional enzymes (*4*−*6*). In *Bacillus subtilis* and a few closely related *bacilli*, a monofunctional RFK encoded by the *ribR* gene is present in addition to the bifunctional RibC, which probably plays a regulatory or supplementary role in flavin cofactor biosynthesis pathways (*7*). Flavin nucleotides (FMN and FAD) are essential cofactors for a large number of flavoproteins that participate in a wide range of metabolic processes. Not surprisingly, genes encoding bifunctional FADS in a number of bacterial species and yeast genes encoding monofunctional RFK (*fmn1*) and FMNAT (*FAD1*) have been shown to be essential for growth and survival of the organisms (*4*, *8*, *9*).

The monofunctional RFK and the RFK domain of the bifunctional FAD synthase comprise a unique protein family, not related to any other kinase or nucleotide binding protein families (*10*). Recently, the crystal structures of both yeast and human RFKs have been determined (*11*, *12*). They revealed a novel kinase fold that contains a six-stranded antiparallel β-barrel core, and unique ATP and flavin binding sites. The ATP binding site of RFK is composed of a glycine-rich loop, a short 3_{10}-helix, and a reverse turn leading to a short β-strand that contains the most conserved PTAN sequence motif. This motif is shown to be intimately involved in the coordination of the Mg^{2+} ion and the binding of the triphosphate moiety of ATP (*11*, *12*). Comparison of yeast apo RFK and the ADP-bound RFK structures showed that the nucleotide binding loop (termed Flap I) mentioned above undergoes drastic conformational changes upon binding of the adenylate nucleotide (*11*). This conformational change also resulted in the stabilization of another loop region (between β-strands **d** and **e**, termed Flap II in ref *11*), which was disordered in the apo RFK structure. The FMN or riboflavin molecule in the enzyme complexes achieved by the soaking experiments exhibited generally good density for the isoalloxazine ring, but poor density for the ribityl side chain, indicating a high degree of flexibility in this region. It is conceivable that for the efficient phosphoryl transfer reaction, the riboflavin ribityl tail needs to be

[†] This work is supported by NIH Grant GM63689 (to H.Z.).

[‡] Protein Data Bank entry 1Q9S.

* To whom correspondence should be addressed. E-mail: zhang@chop.swmed.edu. Phone: (214) 648-9299. Fax: (214) 648-9099.

[§] University of Texas Southwestern Medical Center.

[||] Integrated Genomics, Inc.

[1] Abbreviations: RFK, riboflavin kinase; hsRFK, human riboflavin kinase; spRFK, *Schizosaccharomyces pombe* RFK; FMN, flavin mononucleotide; FAD, flavin adenine dinucleotide; FMNAT, FMN adenylyltransferase; FADS, FAD synthase; TEV, tobacco etch virus; DTT, dithiothreitol.

10.1021/bi035450t CCC: $25.00
Published on Web 10/07/2003

precisely positioned to interact with the γ-phosphate of ATP for the initial in-line attack, a mechanism proposed by Bauer *et al*. (*11*). In both reported human and yeast RFK structures, the ATP/ADP-binding Flap I and the flexible Flap II are involved in extensive interlattice crystal packing interactions. Therefore, it has been hypothesized that conformational changes would be required for the optimal binding of the flavin substrate and/or product, and these conformational changes might involve nearby Flap I and Flap II loops and thus could not be achieved in the previous crystal forms (*11*, *12*).

Here we report the ternary cocrystal structure of human RFK (hsRFK) complexed with both products FMN and MgADP. This complex was crystallized in a different form, and both ligands are well-ordered. Large conformational changes around the substrate binding sites and extensive interactions between the flavin and ATP binding sites are observed. These observations allow us to suggest a structural interpretation of the previously established ordered kinetic mechanism of RFK (*13*, *14*).

EXPERIMENTAL PROCEDURES

Protein Purification and Crystallization. The cloning and expression of human RFK have been described elsewhere (*12*). In the study presented here, the overexpressed protein was first purified with a Ni−NTA affinity column, followed by the TEV protease treatment to cleave the six-His tag. The protease-treated protein was then passed through a second Ni−NTA column to remove the uncleaved enzyme. The hsRFK with the six-His tag removed was dialyzed against a buffer containing 50 mM Tris (pH 7.4), 300 mM NaCl, and 1 mM DTT at 4 °C overnight and then concentrated to 34 mg/mL. In a manner different from the previously reported purification scheme (*12*), we omitted the Phenyl Sepharose chromotography step which would remove the bound FMN from the enzyme. The protein complex purified by this simplified procedure retains both FMN and MgADP and is bright yellow. The crystals were grown at 20 °C by the hanging drop vapor diffusion method. hsRFK (34 mg/mL) was mixed with the same amount of reservoir solution containing 0.1 M sodium acetate (pH 4.7), 30% monomethyl polyethylene glycol (PEG MME) 5000, and 0.2 M $(NH_4)_2SO_4$ and equilibrated against the reservoir. Yellow thin plate crystals appeared in the drop after 3−4 days. The crystals suitable for the diffraction experiment were obtained by microseeding procedure in drops containing 0.1 M sodium acetate (pH 4.4), 22.5% PEG MME 5000, and 0.2 M $(NH_4)_2SO_4$. These crystals were cryoprotected in a solution containing 30% glycerol in addition to the reservoir ingredients, flash-cooled, and stored in liquid propane.

Data Collection, Structure Determination, and Refinement. A complete data set was collected from a single frozen crystal at 100 K on an R-AXIS IV imaging plate detector using Cu Kα radiation from a RIGAKU RU-H3R generator focused with Osmic mirrors. A total of 197 frames were collected, each with an oscillation of 1° and an exposure time of 20 min. The data were processed and scaled using HKL2000 (*15*). The crystal diffracts to 2.4 Å resolution and belongs to space group $C222_1$, with one molecule in the asymmetric unit. The unit cell parameters are as follows: $a = 76.31$ Å, $b = 118.79$ Å, and $c = 37.98$ Å. The structure was determined by the molecular replacement method using AMORE (*16*) and previously reported hsRFK structure (PDB entry 1NB0) (*12*) as a search model with ligands and solvent molecules removed. The rotation function search in the resolution range of 15.0−3.0 Å produced a clean solution with a peak height of 8.2σ above the mean. Subsequent translation function calculation and rigid body refinement yielded a correlation coefficient of 0.456 and an *R*-factor of 45.2%. This model was refined to 2.4 Å using CNS (*17*) and partially rebuilt using O (*18*). The FMN and MgADP molecules were built in the model on the basis of the difference electron densities. Several rounds of simulated annealing and positional and *B*-factor refinement reduced the *R*-factor and R_{free} to 0.26 and 0.32, respectively. At this stage, water molecules were added to the model using the water_pick routine of CNS (*17*), provided they met the criteria of a peak height of 3σ in the difference density and at least making one hydrogen bond with the surrounding atoms with good geometry. After 86 water molecules had been added to the model, the refinement converged to final *R*-factor and R_{free} values of 0.199 and 0.260, respectively. In the final refined model, N-terminal residues 1−6 and C-terminal residues 156−162 could not be located in the electron density and are not included. The data collection and final refinement statistics are given in Table 1.

Table 1: Data Collection and Refinement Statistics

data collection	
space group	$C222_1$
resolution (Å)	50.00−2.4
outer shell (Å)	2.51−2.4
total no. of observations	42992
no. of unique reflections	6912
R_{sym}[a]	0.061 (0.241)[b]
completeness (%)	99.7 (99.5)
redundancy	6.2 (5.8)
average $I/\sigma(I)$	35.5 (7.2)
refinement	
resolution (Å)	35.00−2.4
no. of reflections in the working set	6566
no. of reflections in the test set	330
R_{cryst} (%)[c]	19.9
R_{free} (%)[d]	26.0
no. of non-hydrogen protein atoms	1192
no. of solvent atoms	86
no. of ligand atoms	59
average *B* value for all protein atoms (Å^2)	32.2
average *B* value for all ligand atoms (Å^2)	21.8
average *B* value for all solvent atoms (Å^2)	33.0
rmsd[e] for bond lengths (Å)	0.012
rmsd[e] for bond angles (deg)	1.6

[a] $R_{sym} = \sum|I - \langle I\rangle|/\sum(I)$, where I is the observed integrated intensity and $\langle I\rangle$ is the average integrated intensity obtained from multiple measurements. The summation is over all observed reflections. [b] Values in the parentheses are for the outer resolution shell. [c] $R_{cryst} = \sum||F_{obs}| - k|F_{calc}||/\sum|F_{obs}|$, where F_{obs} and F_{calc} are the observed and calculated structure factors, respectively. [d] R_{free} is calculated as R_{cryst} using 5% of the reflection data chosen randomly and omitted from the refinement calculations (*20*). [e] Root-mean-square deviation from ideal values.

RESULTS AND DISCUSSION

FMN Binding-Induced Conformational Changes. The hsRFK complexed with the intrinsically bound and copurified FMN and MgADP is crystallized in orthorhombic space group $C222_1$, different from that of the previously reported MgADP−enzyme binary complex (space group $P3_121$) (*12*).

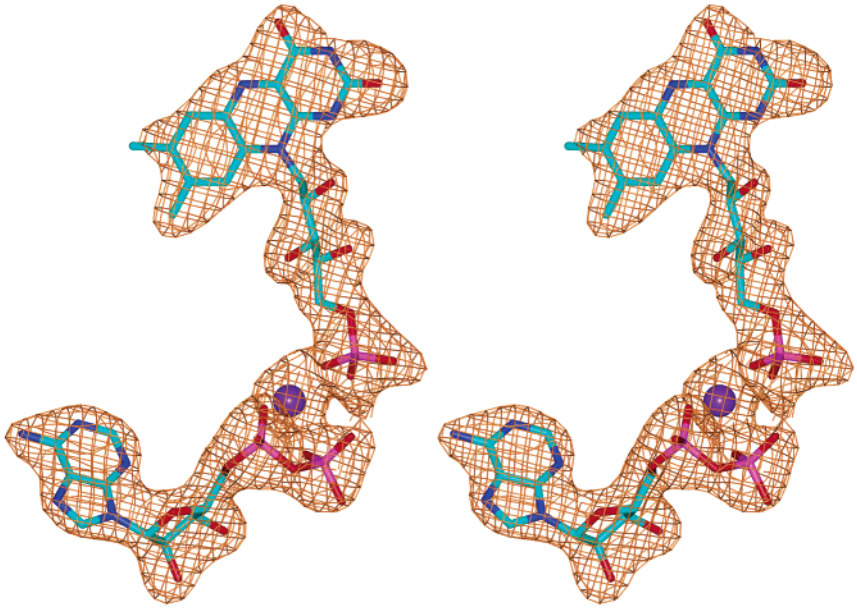

FIGURE 1: Stereoviews of the $F_o - F_c$ omit electron density map for FMN and MgADP. The map is contoured at 3σ. This figure was prepared with Bobscript (*21*) and rendered with gl_render (L. Esser, unpublished program).

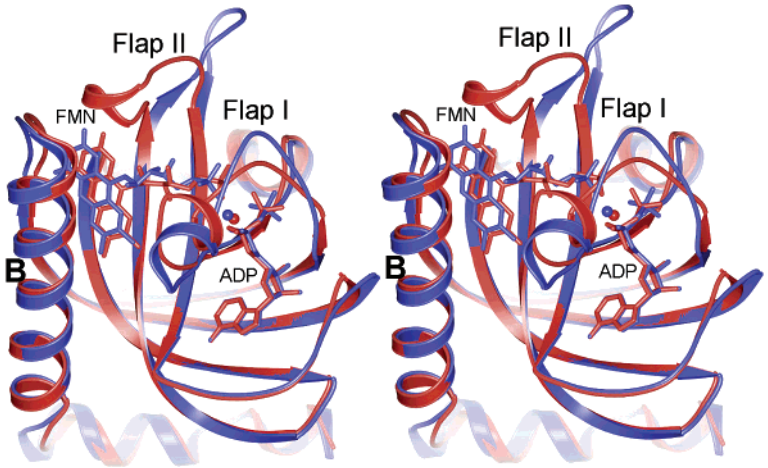

FIGURE 2: Stereoviews of the superposition of the cocrystal ternary product complex structure (red) and the MgADP binary complex soaked with FMN (blue). The ligands (ADP and FMN) are shown as sticks, and Mg^{2+} ion is shown as a ball. Regions termed Flap I, Flap II, and Helix B are labeled. This figure was prepared with Bobscript (*21*) and rendered with gl_render (L. Esser, unpublished program).

The cocrystal structure was determined by the molecular replacement method and refined to 2.4 Å resolution. Both FMN and MgADP molecules in the complex are well-ordered and are represented by unambiguous electron densities (Figure 1). The average *B*-factor of the ligands is 21.8 $Å^2$, comparable to that of the surrounding protein atoms (Table 1), indicating full occupancy for both ligands. Superposition of the cocrystal structure of the ternary product complex with the structure of the binary MgADP complex resulted in a rather large overall rmsd (root-mean-square deviation) of 2.73 Å over all 148 C_α positions in the model. However, the most drastic conformational changes occur primarily at the ADP/ATP-binding Flap I and Flap II regions (Figure 2). When residues in these two regions (22−32 and 74−83) were excluded, the rmsd of the C_α positions decreases to 0.68 Å. Substantial conformational changes also occur in the N-terminal half of Helix B, which is shifted ~1 Å compared to the binary MgADP complex structure. The superposition also reveals that the position of the FMN molecule in the cocrystal is shifted by ~1 Å compared to that in the soaked complex structure (Figure 2). It is clear that all regions that undergo substantial conformational changes in the structure presented here are involved in the interactions with various parts of the bound FMN molecule, and these are described below.

FMN Binding Site. The detailed interactions between the enzyme and FMN molecule in the cocrystal structure are shown in Figure 3. There are extensive hydrophobic interactions between the FMN molecule and the enzyme, as well as several specific hydrogen bond interactions between polar groups of FMN and the protein. Some of these interactions have been observed in the FMN-soaked complex reported previously (*12*), while others can only be achieved in the new crystal form as the result of the conformational changes in the surrounding regions. Specifically, side chains of residues Leu122 and Ile126 from Helix B contact the isoalloxazine ring from above; Ile53 from strand **c** and Val69 and Ser71 from strand **d** buttress the isoalloxazine from underneath and on the side (Figure 3); Asn75 and Tyr78 from Flap II interact with the ribityl portion of FMN mostly

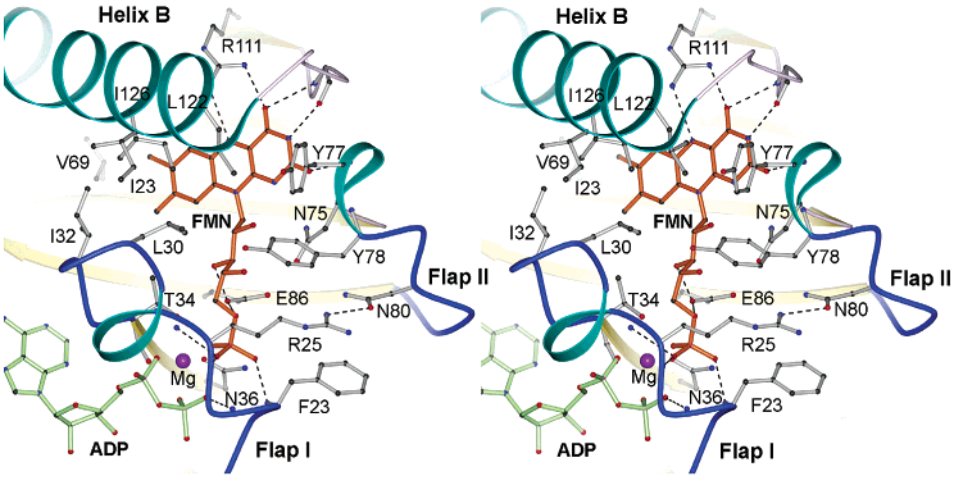

FIGURE 3: Stereoviews of the detailed interactions with FMN in the enzyme−product cocrystal structure. The ligands (MgADP and FMN) and relevant protein residues are shown as a ball-and-stick representation. Flap I, Flap II, and Helix B are labeled. Hydrogen bonds are represented with dashed lines. This figure was prepared with Bobscript (*21*) and rendered with gl_render (L. Esser, unpublished program).

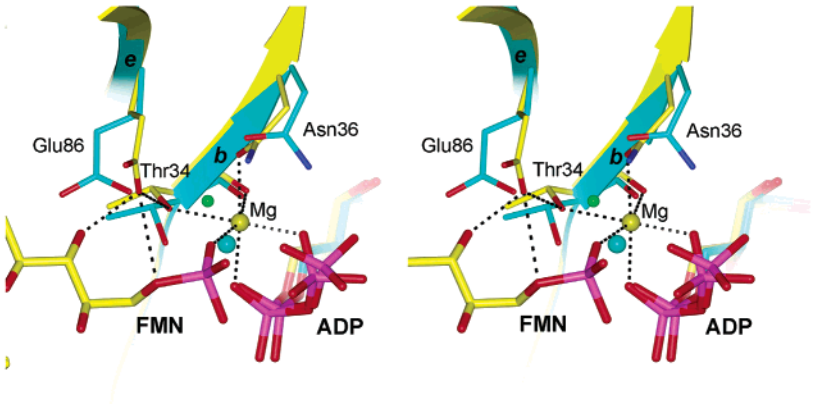

FIGURE 4: Stereoviews of the Mg^{2+} binding site in the product cocrystal structure (yellow) superimposed with that in MgADP binary complex structures (cyan). The hydrogen bonds and metal ion coordination in the cocrystal structure are represented with dashed lines. The water molecule in the MgADP binary complex structure but not in the ternary cocrystal structure is shown as a small green ball. β-Strands **b** and **e** are also labeled. This figure was prepared with Bobscript (*21*) and rendered with gl_render (L. Esser, unpublished program).

through van der Waals contacts. These later interactions are achieved only after the conformational changes of Flap II and are not present in the previously reported "open" structure (*11*, *12*). Specific hydrogen bond interactions include the side chain of Arg111 with O4 and N5 groups, the main chain carbonyl of Lys114 with the N3 group on the FMN isoalloxazine ring, and the Glu86 side chain carboxylate coordinating with the O3′ hydroxyl and the phosphorylated O5′ on the ribityl tail (Figure 3). The large conformational changes in the Flap I region enable extensive interactions between the enzyme and FMN phosphate (Figures 3 and 4). One of the FMN phosphate oxygens is now coordinated with Mg^{2+}. Four consecutive protein main chain amide groups from residues Phe23, Gly24, Arg25, and Gly26, all from the glycine-rich Flap I, form hydrogen bonds with the FMN phosphate. Additionally, the side chain of Leu30 now comes into contact with the FMN ribityl tail as well (Figure 3).

The conformational changes in the Flap I and Flap II regions provided substantially more interactions with both the ribityl tail and the isoalloxazine ring of FMN. These extensive interactions appear to anchor the FMN molecule firmly in the active site and to shield it from the bulk solvent. Notably, the shift in the position of the FMN molecule in the cocrystal structure compared with that of the FMN-soaked complex appears to correlate with the conformational changes of the surrounding protein residues, and reflects a certain fluidity of the FMN binding site.

MgADP Binding Site. As shown in the cocrystal and FMN-soaked hsRFK ternary complex structures, the Flap I region (or the "arch" as in ref *12*) is shared by both flavin and ATP/ADP binding sites, and it interacts extensively with the ADP phosphates as well. The conformation of the ADP molecule in the ternary cocrystal structure remains largely the same as that in the binary MgADP−enzyme complex, except that the positions of the three ADP β-phosphate oxygens are now different (Figure 4). As a result, the number of interactions between Flap I and ADP phosphates remains essentially the same despite large conformational changes in Flap I. In the ternary cocrystal structure, the ADP α-phosphate oxygens interact with main chain amide groups of Ser27 and Thr34; the β-phosphate interacts with the main chain amides of two glycine residues, Gly22 and Gly24, and with the side chain hydroxyl of Tyr98. The Mg^{2+} ion remains coordinated to both α- and β-phosphate oxygens, the side chain hydroxyl and main chain carbonyl of Thr34, which is part of the most conserved PTAN motif on β strand **b**. However, the position of the Mg^{2+} ion in the cocrystal structure is shifted ∼0.9 Å compared to that in the flavin free MgADP−enzyme complex (Figure 4). Because of this shift of the Mg^{2+} ion

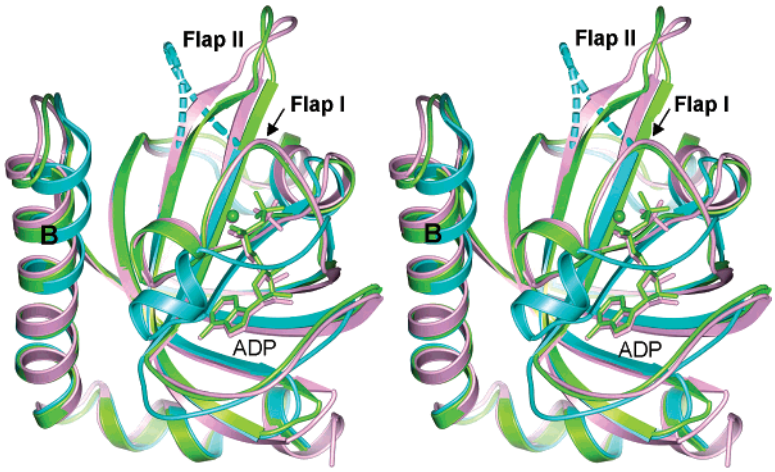

FIGURE 5: Stereoviews of the superposition of hsRFK−MgADP complex structure (magenta) with the yeast apo (cyan) and ADP-bound RFK (green). The MgATP molecule is shown as a ball-and-stick representation. The disordered Flap II region in the yeast apo RFK structure is represented with dashed lines. This figure was prepared with Bobscript (*21*) and rendered with gl_render (L. Esser, unpublished program).

position and a side chain conformational change of Asn36 (also of PTAN motif), the Asn36 side chain is now directly coordinated to Mg^{2+}. The Mg^{2+} coordination position taken by Asn36 was previously occupied by a water molecule, which also interacts with Glu86 and Asn36 side chains in the binary MgADP−enzyme complex (Figure 4). This water molecule is no longer present in the current ternary cocrystal structure.

Clearly, the active site composition in the present ternary cocrystal structure is more catalytically competent than the previous MgADP binary complex structure. Glu86 (and the corresponding Glu96 in yeast RFK) has been hypothesized to play a role as the catalytic base in activating the phosphoryl accepting O5′ hydroxyl group of the riboflavin (*11*, *12*). This Glu86 is well-positioned in the ternary complex to perform such a role (Figure 4). In contrast, in the previous MgADP binary complex structure, the presence of a nearby water molecule may compromise the ability of Glu86 to function as a base. It would also affect the conformation of Glu86 in such a way that the bound riboflavin ribityl side chain could not be positioned optimally (Figure 4). The new Mg^{2+} coordination pattern observed in the current cocrystal structure emphasizes the importance of the invariant Asn36 in catalysis. With the side chain carbonyl directly coordinating to Mg^{2+} ion and the amide group potentially interacting with the γ-phosphate of ATP, Asn36 is centrally positioned at the site where phosphate transfer takes place.

In the product cocrystal structure presented here, flavin binding-induced conformational changes in Flap II lead to its more extensive contact with Flap I. These include the stacking interactions among residues Tyr78, Arg25, and Phe23 and hydrogen bonds between the side chains of Arg25 and Asn80, and Gln29 and Tyr78 (Figure 3). These interactions may stabilize the active site Flap I in a more productive conformation, and help to correctly line up the catalytical residues and the metal ion to facilitate the phosphoryl transfer reaction. At the same time, the close contacts among Flap I, Flap II, and Helix B largely shield the active site from the solvent, thus ensuring a favorable environment for phosphoryl transfer from ATP to the O5′ hydroxyl group of riboflavin.

Comparison with Yeast RFK Structures. Recently, the crystal structures of RFK from *Schizosaccharomyces pombe* (fission yeast) have been determined in the apo as well as in the ADP-bound form (*11*). In both human and yeast RFK−MgADP complex structures, the Flap I has an arch-like appearance with ADP phosphates binding beneath it (Figure 5). However, in the apo spRFK structure, the nucleotide binding Flap I and β-strand **b** adopt a drastically different conformation: together, they collapsed onto the side of the β-barrel core, and Flap I no longer has the arch-like appearance (Figure 5). Combined with the conformational changes in the loop connecting strands **e** and **f** (termed Loop 2 or L2 in ref *12*), the entire ATP binding site is now filled by the proteins atoms almost completely. Additionally, in the yeast apo RFK structure, Flap II is completely disordered and Helix B is positioned toward Flap I with its N-terminal half shifted by as much as 1.8 Å (Figure 5).

Human and yeast RFKs are 44% identical in sequence, and the two ADP-bound enzyme complex structures are very similar (rmsd of C_α positions is 1.2 Å). This conformational similarity is largely retained in the three flexible regions surrounding the substrate binding site, namely, Flap I, Flap II, and Helix B (Figure 5). The metal coordination patterns (Mg^{2+} in hsRFK and Zn^{2+} in spRFK) are also very similar in the two ADP-complexed enzymes. This suggests that the observed conformational changes upon binding of ADP are induced mostly by ligand binding, which causes similar effects in both human and yeast enzymes. It is unlikely that these conformational changes are due to crystal packing artifacts, since human and yeast RFKs were crystallized under different conditions and in different crystal lattices. So far, we have not been able to obtain apo hsRFK crystals, but it may be reasonable to assume that apo hsRFK should adopt a conformation similar to that of yeast apo RFK. Conversely, the conformation of yeast RFK complexed with both products may be similar to that of the human RFK ternary complex as well. So far, a cocrystal structure of RFK complexed with any substrate (ATP, riboflavin, or both) has not been reported. It may be reasonable to assume that the general feature of the active site conformation of the substrate-bound enzyme is more similar to the cocrystal

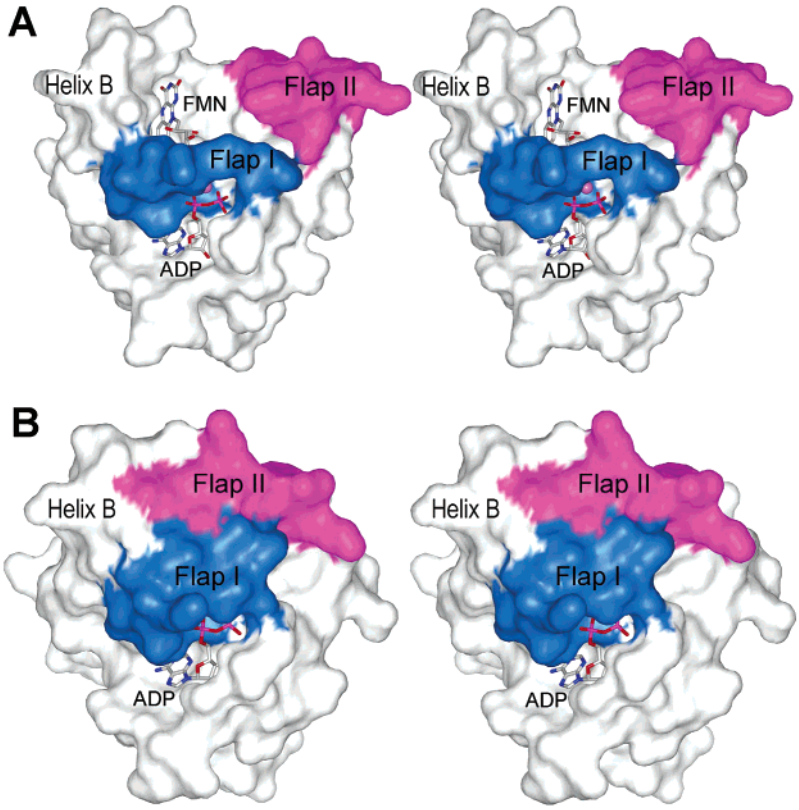

FIGURE 6: Stereoviews of the molecular surfaces of (A) hsRFK complexed with MgADP and with a soaked FMN molecule and (B) hsRFK cocrystallized with MgADP and FMN. The ligands (MgADP and FMN) are shown as sticks. The surface area contributed by residues from the Flap I region is colored blue, and the surface area contributed by residues from the Flap II region is colored magenta. This figure was generated with GRASP (*22*).

structure of the ternary product complex than to the binary MgADP complex, especially because the active site residue arrangement in the cocrystal appears to be more catalytically competent. Understandably, the conformation of Flap I in the enzyme−substrate complex would be somewhat different from that in the enzyme−product complex, since it will interact with ATP triphosphates but not the FMN phosphate.

Implication for the Ordered Mechanism of RFK. For ATP to bind to the apoenzyme, many protein−protein interactions among Flap I, strand **b**, and the β-barrel core will need to be disrupted; new interactions need to be made between ATP, metal ion, and the binding site residues of the enzyme, especially those from Flap I and the PTAN motif on strand **b**. The ATP or ADP binding stabilizes Flap I in the arch-like conformation, which in turn seems to stabilize the conformation of the flavin binding Flap II, as it becomes better ordered in the enzyme−ADP complex (*11*, *12*). Additionally, as a result of the conformational changes in Flap I, the N-terminal end of Helix B is shifted by ~1.8 Å because of its contact with the residues from the short helix on Flap I. In contrast to the extensive rearrangement of protein−protein interactions that are required for binding ATP by the apo RFK, the flavin binding site is open in the apoenzyme structure and the riboflavin molecule should be able to enter the binding site unhindered.

These observations correlate well with the kinetic properties of RFK. Previous kinetic studies of the monofunctional mammalian RFK and the bifunctional bacterial FAD synthase have suggested that both enzymes use an ordered bi-bi mechanism for RFK, in which the preferred pathway is for riboflavin to bind to the enzyme first followed by ATP. Then it is energetically more favorable that product ADP is released first followed by the release of FMN (*13*, *14*). By combining all the structural information obtained so far on the human and yeast RFKs, we may explain such an ordered mechanism at the structure level. In the apo RFK structure, active site Flap I collapsed onto the β-barrel and the ATP binding cavity was no longer there. Accordingly, Flap II is disordered because of a lack of interaction with the surrounding protein atoms (*11*). In this conformational state, the flavin binding site is open while the ATP binding site is closed. Thus, the enzyme would initially prefer binding the flavin substrate first. Binding of the flavin substrate is likely to induce conformational changes in Flap II similar to that induced by the binding of FMN in the present cocrystal structure. Specifically, Flap II closes in on the riboflavin substrate, comes into contact with the N-terminus of Helix B, and probably would also contact Flap I (Figures 3 and 5). This interaction between Flap II and Flap I may induce conformational changes in Flap I and partially open the ATP binding site for the ATP molecule to enter. Since no cocrystals of the substrate complex of RFK have been obtained so far, at this point we can only speculate that the conformation of the active site in the substrate-bound state may adopt a conformation somewhat similar to that of the product cocrystal structure, although the precise conformation of Flap I will likely be different. After the catalysis, as is shown in the ternary product cocrystal structure, the flavin binding site remains completely blocked by Flap II and the product FMN is mostly buried. However, in this state, the ADP site is largely exposed to the solvent; thus, it would be energetically more favorable for ADP to dissociate first from

the enzyme. Release of ADP would induce Flap I to fall back to the "collapsed" conformation like that in the apo state and result in the disordering of Flap II, thus opening the flavin binding site for the FMN molecule to be released.

Together with the data obtained from previous human and yeast RFK complex structures, three distinct conformational states of RFK have now been characterized: the apo form, the ternary product complex, and a relatively unproductive binary MgADP complex. These structures further illustrated the unique features of substrate binding and catalysis of the enzyme. Large conformational changes, primarily occurring on two surface loops (Flaps I and II), accompany the binding of each substrate. The preferred order of substrate binding and product release appears to be directly related to the energetics associated with these conformational changes. Our current cocrystal structure also revealed a different Mg^{2+} ion coordination pattern which emphasizes the potential catalytical role of the invariant Asn36 residue.

As we were preparing this paper, the crystal structure of the putative bifunctional FAD synthase from *Thermotoga maritima* was reported (*19*). In this apo form FADS structure, both Flap I and Flap II regions of the RFK domain are disordered. It appears that although RFKs from different organisms share a high degree of sequence similarity and similar kinetic properties (*13*, *14*), there may be variations in the detailed structural mechanisms for substrate binding and catalysis. Further structural and biochemical studies will be necessary to fully understand the dynamics and detailed conformational changes along the reaction coordinate.

ACKNOWLEDGMENT

We thank Faika Mseeh for cloning hsRFK and Nick Grishin for stimulating discussion and critical reading of the manuscript.

REFERENCES

1. Bacher, A. (1991) in *Chemistry and biochemistry of flavoenzymes* (Müller, F., Ed.) Vol. 1, pp 349−370, CRC Press, Boca Raton, FL.
2. Manstein, D. J., and Pai, E. F. (1986) *J. Biol. Chem. 261*, 16169−16173.
3. Mack, M., van Loon, A. P., and Hohmann, H. P. (1998) *J. Bacteriol. 180*, 950−955.
4. Santos, M. A., Jimenez, A., and Revuelta, J. L. (2000) *J. Biol. Chem. 275*, 28618−28624.
5. Kasai, S., Nakano, H., Maeda, K., and Matsui, K. (1990) *J. Biochem. 107*, 298−303.
6. Merrill, A. H., Jr., and McCormick, D. B. (1980) *J. Biol. Chem. 255*, 1335−1338.
7. Solovieva, I. M., Kreneva, R. A., Leak, D. J., and Perumov, D. A. (1999) *Microbiology 145*, 67−73.
8. Gerdes, S. Y., Scholle, M. D., D'Souza, M., Bernal, A., Baev, M. V., Farrell, M., Kurnasov, O. V., Daugherty, M. D., Mseeh, F., Polanuyer, B. M., Campbell, J. W., Anantha, S., Shatalin, K. Y., Chowdhury, S. A., Fonstein, M. Y., and Osterman, A. L. (2002) *J. Bacteriol. 184*, 4555−4572.
9. Wu, M., Repetto, B., Glerum, D. M., and Tzagoloff, A. (1995) *Mol. Cell. Biol. 15*, 264−271.
10. Cheek, S., Zhang, H., and Grishin, N. V. (2002) *J. Mol. Biol. 320*, 855−881.
11. Bauer, S., Kemter, K., Bacher, A., Huber, R., Fischer, M., and Steinbacher, S. (2003) *J. Mol. Biol. 326*, 1463−1473.
12. Karthikeyan, S., Zhou, Q., Mseeh, F., Grishin, N. V., Osterman, A. L., and Zhang, H. (2003) *Structure 11*, 265−273.
13. Yamada, Y., Merrill, A. H., Jr., and McCormick, D. B. (1990) *Arch. Biochem. Biophys. 278*, 125−130.
14. Efimov, I., Kuusk, V., Zhang, X., and McIntire, W. S. (1998) *Biochemistry 37*, 9716−9723.
15. Otwinowski, Z., and Minor, W. (1997) *Methods Enzymol. 276*, 307−326.
16. Navaza, J. (1994) *Acta Crystallogr. A50*, 157−163.
17. Brünger, A. T., Adams, P. D., Clore, G. M., DeLano, W. L., Gros, P., Grosse-Kunstleve, R. W., Jiang, J. S., Kuszewski, J., Nilges, M., Pannu, N. S., Read, R. J., Rice, L. M., Simonson, T., and Warren, G. L. (1998) *Acta Crystallogr. D54*, 905−921.
18. Jones, T. A., Zou, J.-Y., Cowan, S. W., and Kjeldgaard, M. (1991) *Acta Crystallogr. A47*, 110−119.
19. Wang, W., Kim, R., Jancarik, J., Yokota, H., and Kim, S.-H. (2003) *Proteins 52*, 633−635.
20. Brünger, A. T. (1992) *Nature 355*, 472−475.
21. Esnouf, R. (1997) *J. Mol. Graphics Modell. 15*, 133−138.
22. Nicholls, A. (1993) *Grasp: Graphical Representation and Analysis of Surface Properties*, Columbia University, New York.

BI035450T